Supplementary Information for

A Type of B←N-embedded Molecule Used as Cathode Interlayer Enables Enhanced Open-circuit Voltage

Zixin Liu, [a] *Weibin Chen,* [a] *Zhengxi Ning,* [a] *Nuo Xu* [a] *and Jianhua Huang** [a]

[a] *College of Materials Science and Engineering, Huaqiao University, Xiamen 361021, China.*

Contents

1. Experimental section

1.1 Materials, instruments, and measurements

All commercially available chemicals were used without further purification unless otherwise noted. D18, PM6, L8-BO, Y6, PFN-Br, and PDINN were purchased from Detron, Shenzhen. Tetrahydrofuran was distilled freshly from sodium benzophenone ketyl under nitrogen before use. Column chromatography was performed with silica gel (200-300 mesh). Analytical thin-layer chromatography (TLC) was performed on 0.2 mm silica gel-coated glass sheets with F254 indicator. All yields given referred to isolated yields. Nuclear Magnetic Resonance (NMR) spectra were recorded on Bruker Avance III 500 MHz NMR spectrometers at 298 K. Chemical shifts were reported in ppm. ^{1}H NMR chemical shifts were referenced to TMS (0 ppm), $CDCl_3$ (7.26 ppm). The ^{11}B NMR spectra samples were tested in the quartz NMR tube with boron content lower than 0.1 ppm.

UV-vis absorption was recorded on a Shimadzu UV-2100 spectrophotometer (200–800 nm). Photoluminescence spectra were recorded on an Edinburgh FLS1000 spectrometer. The film samples of OBNP used for absorption and emission spectra were prepared by spin-coating the OBNP solutions (in chloroform, 5 mg/mL) on quartz substrates. Cyclic voltammetry (CV) was carried out in 0.1 M *n*-Bu_4NPF_6 deoxygenated solution in chloroform using a three-electrode configuration (glassy carbon as working electrode, Pt as counter electrode, and saturated calomel electrode as pseudo-reference) and a CHI660e electrochemical workstation. The solutions were bubbled with argon for 5 min prior to the test. The ferrocene/ferrocenium (Fc/Fc^+) couple was served as external reference. The materials were dissolved in the electrolyte at a concentration of 1 mg/mL for measurements. The scanning rate was 100 mV/s. The working electrode was polished with a 0.05 μm alumina paste and washed with water, ethanol and dichloromethane before use. The HOMO and LUMO were estimated using $E_{HOMO/LUMO}$ = -(4.4 + $E_{ox/red}$) eV, where $E_{ox/red}$ is the onset potential of oxidation/reduction processes. Atomic force microscope (AFM) was performed on a Nanoscope V AFM (Digital Instruments) in tapping mode. Scanning Kelvin probe microscopy (SKPM) measurements were carried out in air conditions (using Bruker Multimode 8 instrument) to probe the contact potential difference (CPD) between the surface of organic solar cells and the probe. The samples were prepared by spin-coating CIL solutions on the ITO/PEDOT: PSS/D18: L8-BO substrates. The Kelvin probe of SCM-PIT-V2 was used. Nap mode (Electrical & Magnetic; Electrical & Magnetic Lift Mode) was adopted and direct-current (DC) voltage was applied to the samples. The surface potential (V_{sp}) is defined as $V_{sp} = V_t - V_s$, where V_t and V_s are the potentials of tip and sample, respectively. The Ultraviolet photoelectron spectroscopy (UPS) spectra were collected using a Thermo Fisher Scientific Nexsa at a bias of -5 V using a He-I_α (21.22 eV) UV light source. The UPS samples were

prepared by evaporating the Ag layer (100 nm) on ITO and then spin-coating CIL solutions in methanol (1 mg/mL) onto the ITO/Ag substrates. Another set of UPS samples were prepared by spin-coating BHJ (D18: L8-BO) on ITO substrate and further coating OBNP on the BHJ. XPS tests were conducted on Thermo Scientific K-Alpha. XPS samples were prepared by evaporating the Ag layer (100 nm) on glass substrates and then spin-coating CIL solutions in methanol (1 mg/mL) onto the glass/Ag substrates.

1.2 Theoretical simulations

Density functional theory (DFT) calculations were performed using the Gaussian 09 program with the B3LYP exchange-correlation functional.[1] All-electron triple-ξ valence basis sets with polarization functions (6-31G (d, p)) are used for all atoms. Geometry optimizations were performed with full relaxation of all atoms. Various conformations with different dihedral angles were optimized, and the data for the one with the lowest energy are reported. The electrostatic potential surface (EPS) maps were exported from fchk files on Gaussian view linked to Gaussian 09 program.

1.3 Contact angle tests

The contact angle tests were carried out on the JC2000D measuring instrument. The purpose was to test the wettability of each individual sample and then obtain the compatibility among the samples. Three molecules were respectively dissolved in chloroform solutions (with a concentration of 20 mg/mL), and then spin-coated into films at a relatively low rotation speed (2000 rpm) and attached to the quartz substrates with PEDOT: PSS to prepare samples. Ethylene glycol and distilled water were respectively selected for the wettability tests. According to the test results, the surface tension values of the films could be obtained by Wu's method.[2] And with the obtained above parameters, the interfacial surface energy of the two materials could be deduced by Neumann's equation.[3]

$$\gamma_{water}(cos\theta_{water}+1)=\frac{4\gamma_{water}^{d}\cdot\gamma^{d}}{\gamma_{water}^{d}+\gamma^{d}}+\frac{4\gamma_{water}^{p}\cdot\gamma^{p}}{\gamma_{water}^{p}+\gamma^{p}}$$

$$\gamma_{EG}(cos\theta_{EG}+1)=\frac{4\gamma_{EG}^{d}\cdot\gamma^{d}}{\gamma_{EG}^{d}+\gamma^{d}}+\frac{4\gamma_{EG}^{p}\cdot\gamma^{p}}{\gamma_{EG}^{p}+\gamma^{p}}$$

$$\gamma=\gamma^{d}+\gamma^{p}$$

$$\gamma_{X-Y}=\gamma_{X}+\gamma_{Y}-2\left(\sqrt{\gamma_{X}}\sqrt{\gamma_{Y}}\right)exp[-\delta(\gamma_{X}-\gamma_{Y})^{2}]$$

Among them, θ refers to the contact angle of each film, and γ is the surface free energy of the sample, which is equal to the sum of the dispersive (γ_d) and polar (γ_p) components; γ_{water} and γ_{EG} are the surface tensions of water and ethylene glycol respectively. γ_{water}^{d}, γ_{water}^{p}, γ_{EG}^{d} and γ_{EG}^{P} are the dispersive and polar components of γ_{water} and γ_{EG} respectively. $\delta = 0.0001115\ m^4 \cdot mJ^{-2}$

1.4 Fabrication and tests of photovoltaic devices

The organic solar cells prepared in this work are composed of

ITO/PEDOT:PSS/active layer/CIL/Ag, and the effective area of each device is 0.04 cm^2. The preparation process is as follows: The commercially purchased indium tin oxide (ITO) conductive glass was wiped and cleaned on both sides with detergent, deionized water, acetone, and isopropanol successively. After each wiping, ultrasonic treatment was carried out for 15 minutes. After cleaning, the residual solvents were blown away with nitrogen. Then, the ITO glass with the front side facing up was placed in an ultraviolet-ozone cleaner for 30 minutes to remove the residual oxides on the surface, reduce the work function, and increase the hydrophilicity. After the surface treatment, the anode transport layer PEDOT:PSS was spin-coated onto the ITO glass at a rotation speed of 3000 rpm using a Heraeus Clevios P VP AI 4083 spin coater. The rotation duration was set to 30 seconds. After spin coating, it was annealed on an electric heating plate with the temperature set at 150 °C for 15 min. The active layer was prepared by mixing the donor and the acceptor at a ratio of 1:1.2, dissolving them in chloroform (CF) at a concentration of 15 mg/ml, and then stirring for 3 hours. After that, the active layer solution was spin-coated on top of ITO/PEDOT:PSS surface in a glove box filled with nitrogen atmosphere. During this process, the device processing conditions can be changed for process optimization. After the preparation of the active layer, an cathode interlayer (CIL), e.g., OBNP, PFN-Br, and PDINN with a film thickness of about 10 nm was coated (with a concentration of 1 mg/ml, the solvent being a solution of methanol, the commonly used rotation speed being 3000 rpm, and the rotation time being 40 seconds). The thickness of OBNP in devices was estimated using the extrapolation method by testing the absorption spectra of OBNP films with different thicknesses (Figure S18). The film thickness was tested on a KLA－Tencor/D－600. The CIL-free devices with methanol-treated active layers were also prepared for comparison. Finally, 100 nm of metal Ag was deposited by vacuum evaporation under 4×10^{-5} Pa. After the device preparation was completed, it was transferred to the testing glove box using a transfer shuttle.

Subsequently, the prepared all-polymer solar cells were characterized using a Newport solar simulator. Under the condition of AM 1.5G (100 $mW\bullet cm^{-2}$), the current density-voltage (*J-V*) curves were measured in air using a Keithley 2400 source meter. The light intensity used was calibrated with a standard Si diode (with a KG5 filter, purchased from PV Measurement to unify the spectral mismatch). Monochromatic light was generated by a Newport 300W light source. The device area defined by the Mask was 4 mm^2. The external quantum efficiencies (EQEs) were measured using an Enlitech QE-S EQE system equipped with a standard silicon diode.

1.5 SCLC tests

The electron mobilities were measured by using the method of space-charge limited current (SCLC) for electron-only devices with the structure of ITO/titanium (diisopropoxide) bis(2,4-pentanedionate) (TIPD)/D18: L8-BO/CIL/Al. The TIPD buffer layer was prepared by spin-coating a 3.5 wt % TIPD isopropanol solution onto the pre-cleaned ITO substrate and then baked at 150 °C for 10 min to convert TIPD into TOPD.[4] Subsequently, the blend was spin-coated on it under the same condition as preparation of the optimal solar cell. The CIL layer was spin coated using OBNP,

PFN-Br, or PDINN. A control device without CIL but with methanol-treated active layer was also prepared for comparison. The Al layer was thermally deposited on the top of the blend in vacuum at a speed of 1 Å/ s. The electron and hole mobilities were extracted by fitting the current density-voltage curves using the Mott-Gurney law,[5]

$$J_{SCL} = (9\varepsilon\varepsilon_0\mu V)^2/(8L^3)$$

where ε is the dielectric constant of the organic component, ε_0 is the permittivity of the vacuum (8.85419×10^{-12} C•V^{-1}•m^{-1}), μ is the zero-field mobility, J_{SCL} is the current density, L is the thickness of the active layer, and $V = V_{app} - V_{bi}$, here V_{app} is the applied potential, and V_{bi} the built-in potential which results from the difference in the work function values of the cathode. From the plot of $J^{1/2}$ versus V, the electron mobilities can be deduced.

1.6 Conditivity measurements

The solution of the electron transport layer was spin-coated onto the ITO glass substrate, and then parallel silver electrodes were deposited on the electron transport layer. Electrical characterization was carried out using a probe station equipped with a Keithley 4200 SCS under a nitrogen atmosphere. The conductivity was calculated using the following equation:

$$\sigma = \frac{I \cdot L}{V \cdot W \cdot T}$$

Among them, σ represents conductivity; I represents the measured current; V represents the applied voltage; W represents the length of the silver electrode; L represents the separation distance between the two electrodes, and T represents the thickness of the organic layer.

1.7 Energy loss (E_{loss}) analysis

The E_{loss} is quantified according to the following equation:

$$E_{loss} = (E_g - qV_{oc}^{sq}) + (qV_{oc}^{sq} - qV_{oc}^{rad}) + (qV_{oc}^{rad} - qV_{oc}) = \Delta E_1 + \Delta E_2 + \Delta E_3$$

(1) $\Delta E_1 = E_g - qV_{oc}^{sq}$ represents the unavoidable radiative loss originating from absorption above the bandgap. The is the maximum voltage based on the Schockley-Queisser (SQ) limit:

$$V_{oc}^{sq} = \frac{kT}{q} ln(\frac{J_{sc}^{sq}}{J_0^{sq}} + 1) \cong \frac{kT}{q} ln(\frac{q\int_{E_g}^{+\infty} \varphi_{AM1.5G}(E)dE}{q\int_{E_g}^{+\infty} \varphi_{BB}(E)dE})$$

E_g represents the bandgap of the blend film and q is the elementary charge. $\varphi_{BB}(E)$ is the black body spectrum at 300 K. E_g can be estimated via the derivatives of the sensitive EQE (sEQE) spectra (P(E)=dEQE/dE) as following (Figure S22):

$$E_g = \frac{\int_a^b E_g P(E_g) dE_g}{\int_a^b P(E_g) dE_g}$$

(2) $\Delta E_2 = (qV_{oc}^{sq} - qV_{oc}^{rad})$ can be regarded as radiative loss caused by abosrption below the bandgap, where the V_{oc}^{rad} is the open circuit voltage when there is only radiative recombination. The radiative recombination limit for saturation current (J_0^{rad}) is also calculated from the EQE spectrum.

$$V_{oc}^{rad} = \frac{kT}{q} ln(\frac{J_{sc}}{J_0^{rad}} + 1) \cong \frac{kT}{q} ln(\frac{q\int_0^{+\infty} EQE(E)\varphi_{AM1.5G}(E)dE}{q\int_0^{+\infty} EQE(E)\varphi_{BB}(E)dE}$$

(3) $\Delta E_3 = qV_{oc}^{rad} - qV_{oc}$ can be directly calculated while the other two parts were determined. ΔE_3 Can also be confirmed by measuring the EQE of electroluminescence (EQE_{EL}) of the solar cell through the equation of: $\Delta E_3 = -kTln(EQE_{EL})$. For the EQE_{EL} measurements, a digital source meter (Keithley 2400) was employed to inject electric current into the solar cells, and the emitted photons were collected by a Si diode (Hamamatsu s1337-1010BQ) and indicated by a picoammeter (Keithley 6482).

1.8 Materials synthesis

Synthesis of OBNP. To a stirred solution of 2-(pyridin-2-yl)phenol (200 mg, 1.17 mmol) in dry THF (10 mL), triphenylborane (283 mg, 1.17 mmol) was added. Next, the solution was sealed and stirred at 70 ºC overnight. After cooled to room temperature, the solvent was removed and the resulting solid was re-crystallized from CH_2Cl_2/n-hexane to obtain yellow solid 313 mg (yield 80%). ^{1}H NMR (500 MHz, CD_3Cl) δ 8.16 (m, 1H), 7.99-7.93 (m, 2H), 7.61 (m, H), 7.31 (m, 1H), 7.27-7.20 (m, 12H), 6.84 (m, 1H). ^{11}B NMR (160 MHz, $CDCl_3$) δ 6.05 ppm.

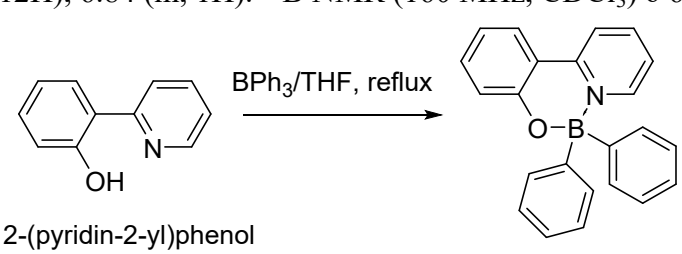

2-(pyridin-2-yl)phenol

OBNP

2 Supporting Figures and Tables

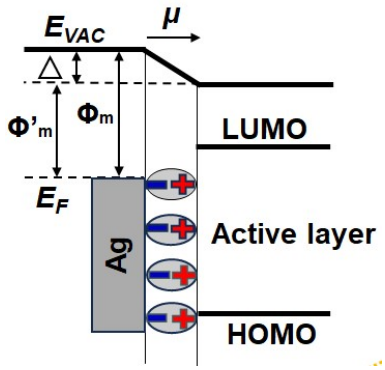

Figure S1. The mainstream work mechanism of CILs by decreasing the metal work function (Φ_m).

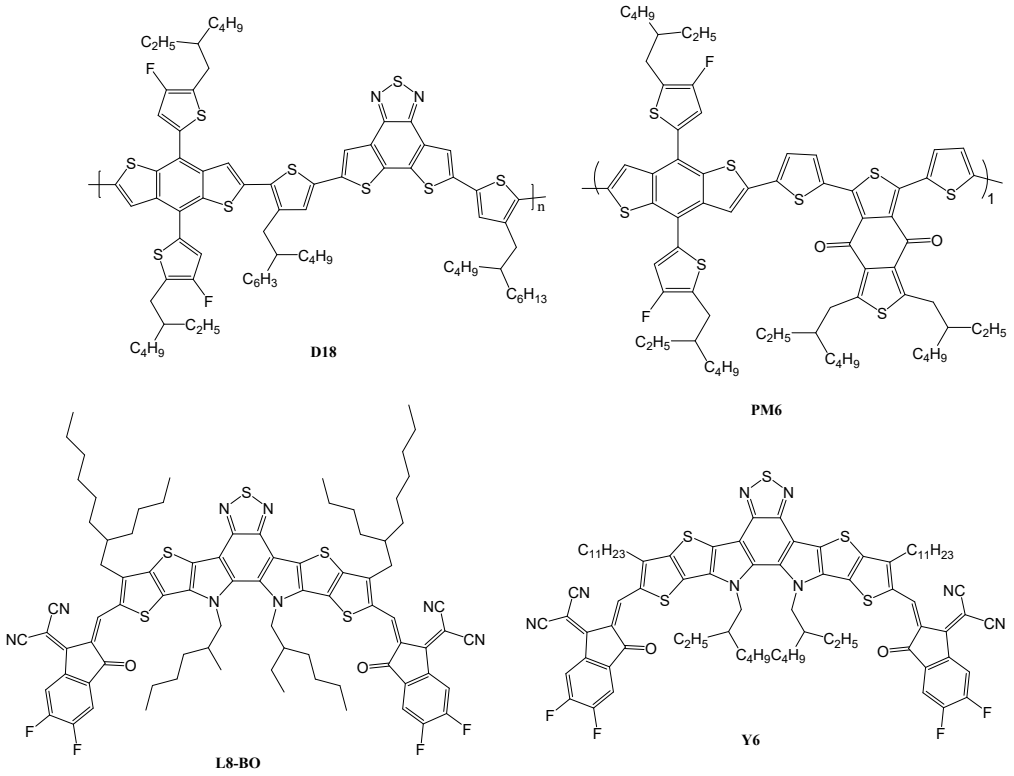

Figure S2. Molecular structures of commercialized donors and acceptors used in this work.

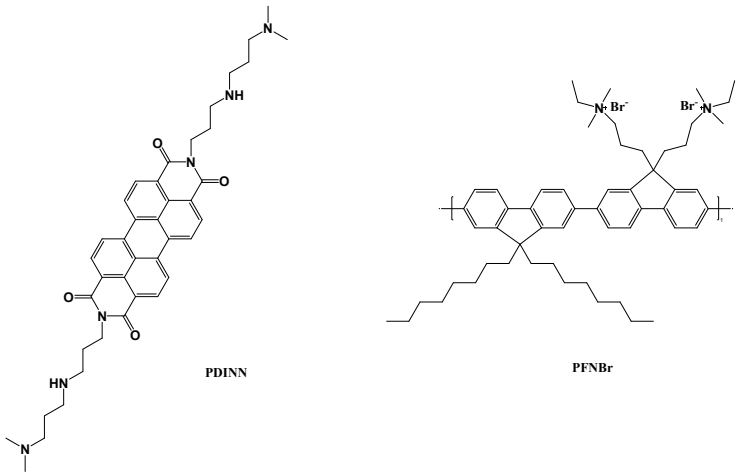

Figure S3. Molecular structures of commercialized CILs used in this work.

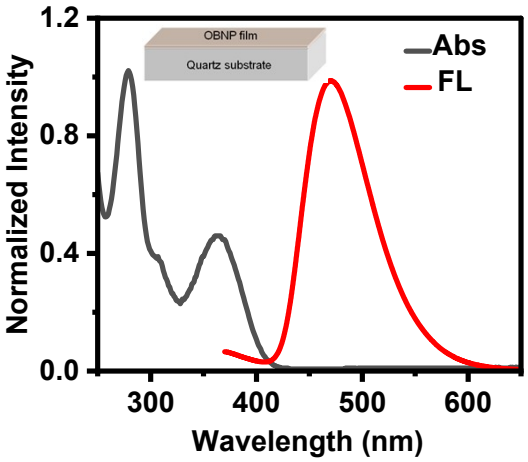

Figure S4. Absorption and emission spectra of OBNP in film.

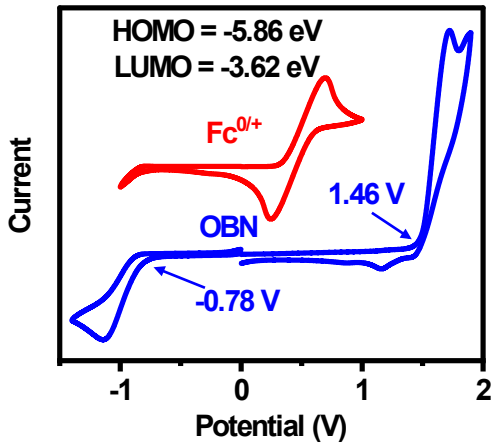

Figure S5. CV curve of OBNP and the calculated HOMO/LUMO energy levels.

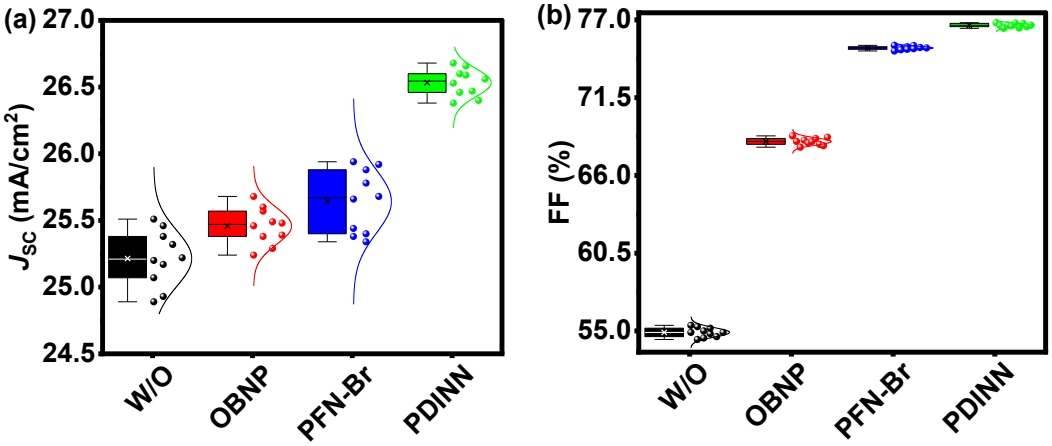

Figure S6. Statistical distribution of J_{SC} and FF values collected from 10 devices based on D18: L8-BO as active layer and different CILs.

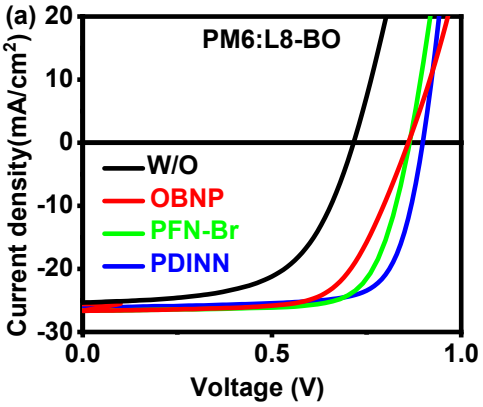

Figure S7. *J-V* curves of devices using PM6: L8-BO as the active layer and different CILs.

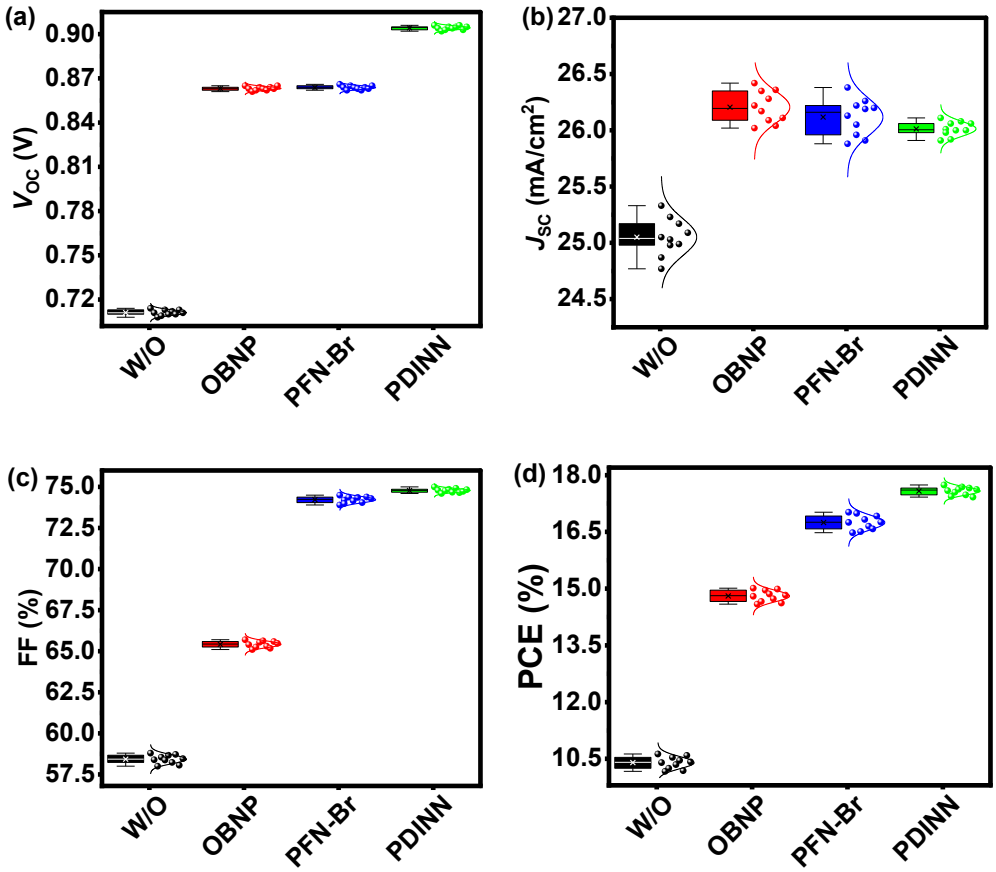

Figure S8. Statistical distribution of V_{OC}, J_{SC}, FF, and PCE collected from 10 devices using PM6: L8-BO as active layer and different CILs.

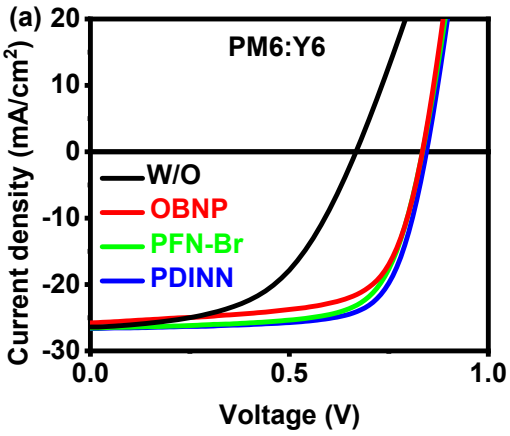

Figure S9. *J-V* curves of devices using PM6: Y6 as the active layer and different CILs.

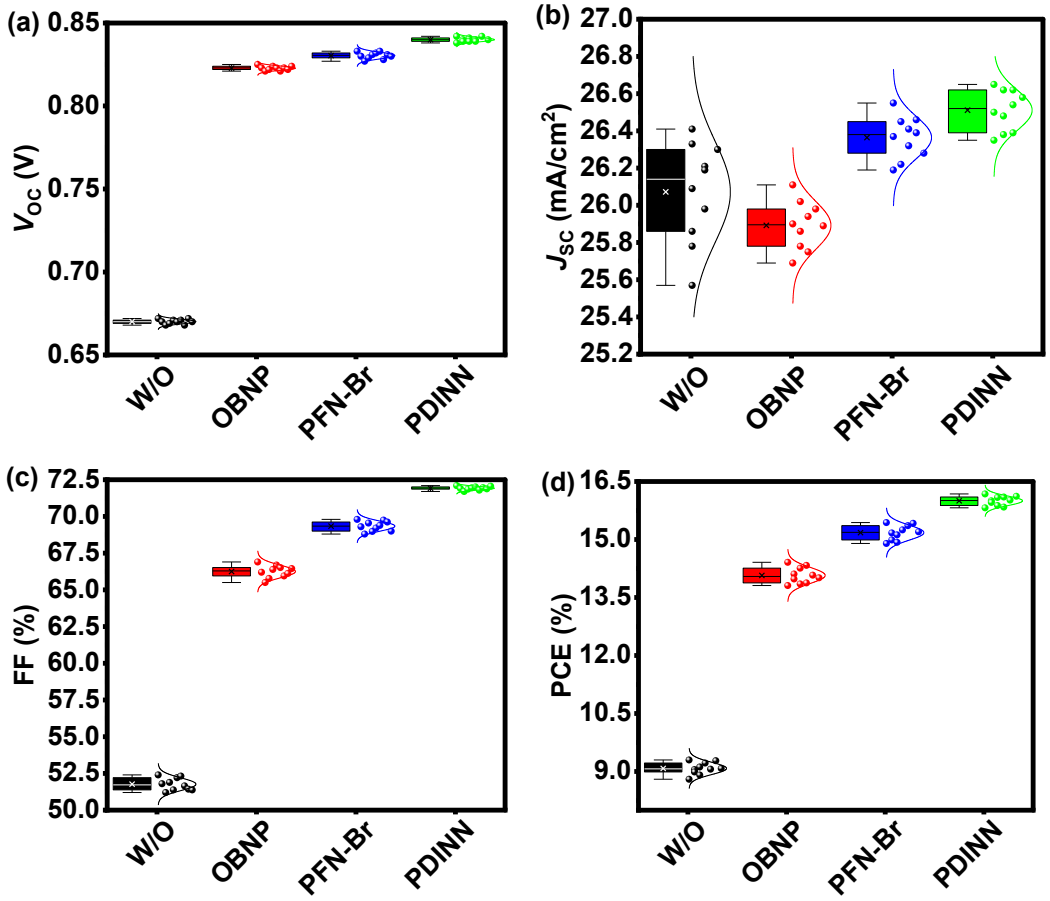

Figure S10. Statistical distribution of V_{OC}, J_{SC}, FF, and PCE collected from 10 devices using PM6: Y6 as active layer and different CILs.

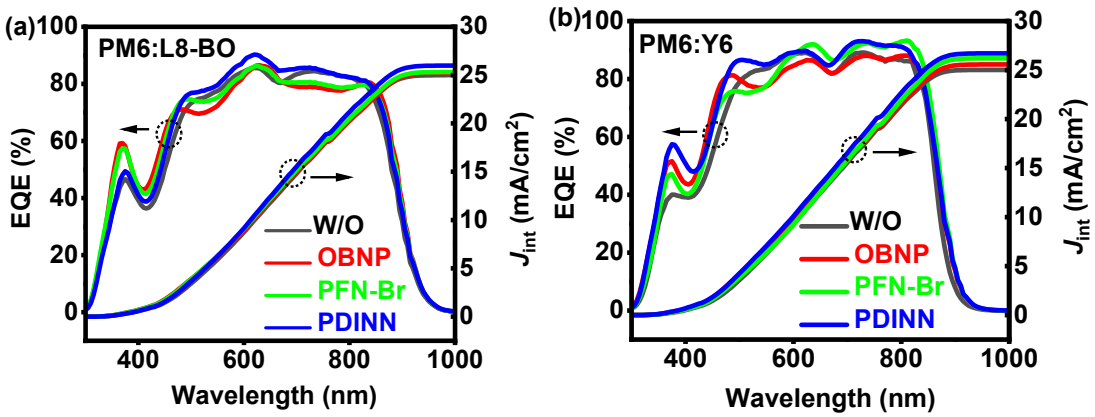

Figure S11. EQE curves of devices using PM6: L8-BO (a) and PM6: Y6 (b) as the active layers and different CILs.

Table S1. Photovoltaic parameters of devices using D18: L8-BO as active layer and different CILs.

CILs	V_{OC} (V)	J_{SC} (mA/cm^2)	J_{Int} (mA/cm^2)	FF (%)	PCE (%)
W/O	0.763 [0.758±0.005]	25.51 [25.20±0.31]	24.40	55.4 [54.9±0.5]	10.78 [10.49±0.29]
OBN	0.882 [0.879±0.003]	25.68 [25.46±0.22]	25.10	68.8 [68.4±0.4]	15.58 [15.31±0.27]
PFN-Br	0.875 [0.873±0.002]	25.94 [25.66±0.28]	25.70	75.2 [75.0±0.2]	17.07 [16.80±0.27]
PDINN	0.904 [0.901±0.003]	26.68 [26.53±0.15]	26.12	76.8 [76.6±0.2]	18.52 [18.31±0.21]

Notes: The averaged values are collected from 10 devices; J_{int} is the integrated current density deduced from EQE curves.

Table S2. Photovoltaic parameters of devices using PM6: L8-BO as active layer and different CILs.

CILs	V_{OC} (V)	J_{SC} (mA/cm^2)	J_{Int} (mA/cm^2)	FF (%)	PCE (%)
W/O	0.714 [0.711±0.003]	25.33 [25.05±0.28]	25.08	58.8 [58.4±0.4]	10.63 [10.40±0.23]
OBN	0.865 [0.863±0.002]	26.42 [26.22±0.20]	25.15	65.7 [65.4±0.3]	15.01 [14.80±0.21]
PFN-Br	0.866 [0.864±0.002]	26.38 [26.13±0.25]	25.40	74.5 [74.2±0.3]	17.02 [16.75±0.27]
PDINN	0.906 [0.904±0.002]	26.11 [26.01±0.10]	26.01	75.0 [74.8±0.2]	17.74 [17.59±0.15]

Notes: The averaged values are collected from 10 devices; J_{int} is the integrated current density deduced from EQE curves.

Table S3. Photovoltaic parameters of devices using PM6: Y6 as active layer and different CILs.

CILs	V_{OC} (V)	J_{SC} (mA/cm^2)	J_{Int} (mA/cm^2)	FF (%)	PCE (%)
W/O	0.672 [0.670±0.002]	26.41 [26.09±0.32]	25.01	52.4 [51.8±0.6]	9.30 [9.05±0.25]
OBN	0.825 [0.823±0.002]	26.11 [25.90±0.21]	25.60	66.9 [66.2±0.7]	14.41 [14.11±0.30]
PFNBr	0.833 [0.830±0.003]	26.55 [26.37±0.18]	26.22	69.8 [69.3±0.5]	15.44 [15.17±0.27]
PDINN	0.842 [0.840±0.002]	26.65 [26.50±0.15]	26.70	72.1 [71.9±0.2]	16.18 [16.00±0.18]

Notes: The averaged values are collected from 10 devices; J_{int} is the integrated current density deduced from EQE curves.

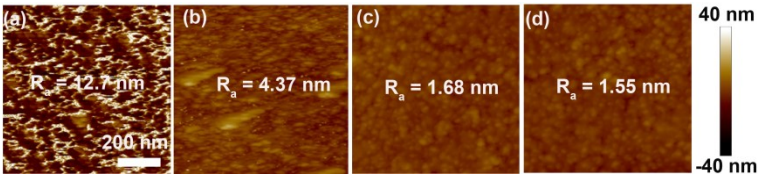

Figure S12, AFM height images of bare Ag (a), Ag/OBNP (b), Ag/PFN-Br (c), and Ag/PDINN (d).

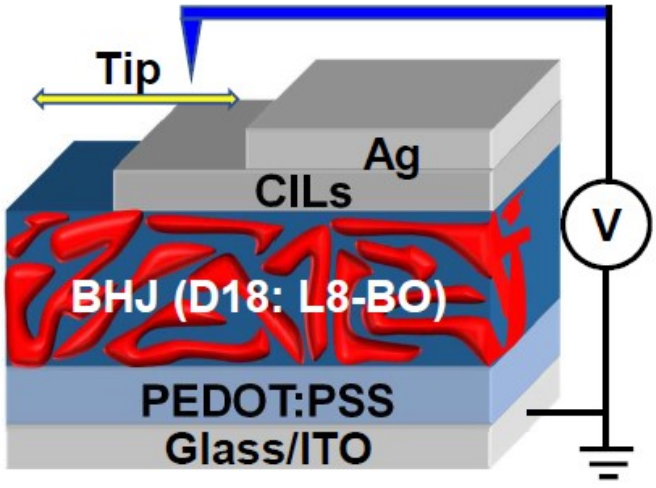

Figure S13. Experimental setup of SKPM.

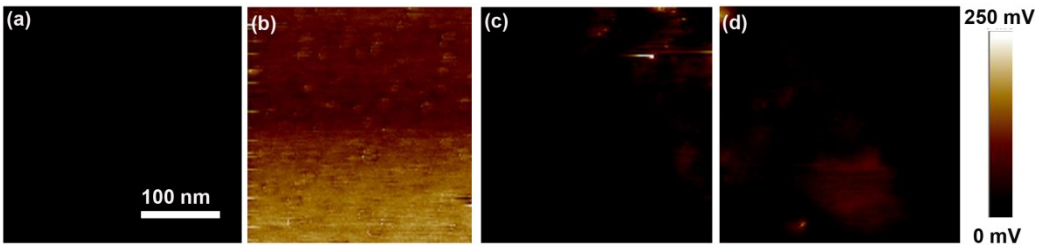

Figure S14. The 2D potential patterns of SKPM measurements for bare BHJ (a), BHJ/OBNP (b), BHJ/PFN-Br (c), and BHJ/PDINN (d).

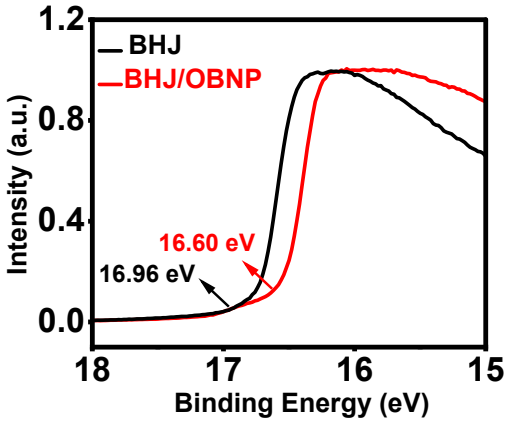

Figure S15. UPS of bare BHJ and BHJ/OBNP.

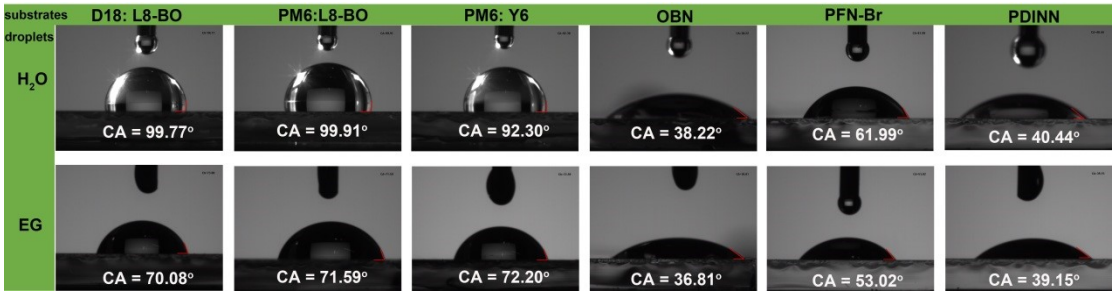

Figure S16. Contact angles of water and ethylene glycol droplets on the different BHJ and CIL surfaces.

Table S4. contact angles and surface energy of different BHJ blends and CILs.

	H_2O (°)	EG (°)	γ_s (mJ/m^2)
D18:L8-BO	94.77	73.08	19.18
PM6:L8-BO	99.91	71.59	18.97
PM6:Y6	92.30	72.20	20.19
OBN	38.22	36.81	63.90
PFN-Br	61.99	53.02	51.30
PDINN	40.44	39.15	60.30

Table S5. Interfacial energy between BHJ blends and CILs

	$\gamma_{interface}$(mJ/m^2)		
	OBN	**PFN-Br**	**PDINN**
D18:L8-BO	25.5	13.2	20.5
PM6:L8-BO	27.3	14.7	22.3
PM6:Y6	24.6	12.4	20.8

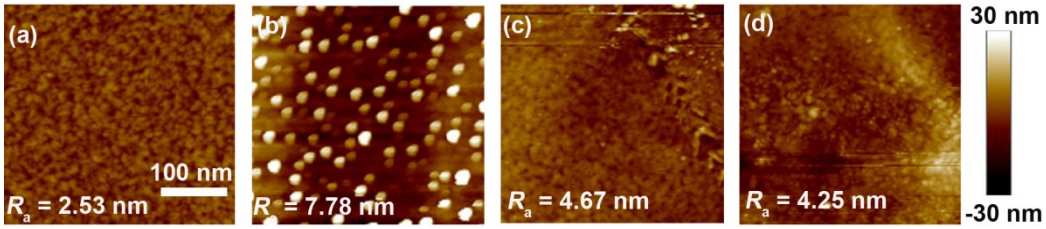

Figure S17. AFM height images of bare BHJ (D18: L8-BO) (a) and BHJ coated by OBNP (b), PFN-Br (c), and PDINN (d).

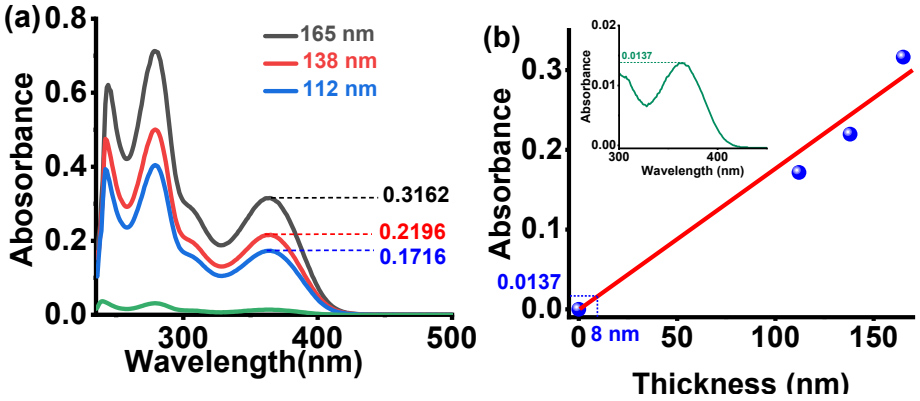

Figure S18. Absorption of OBNP at different film thicknesses (a) and linear fitting of film thickness to absorption to estimate the thickness in device (b).

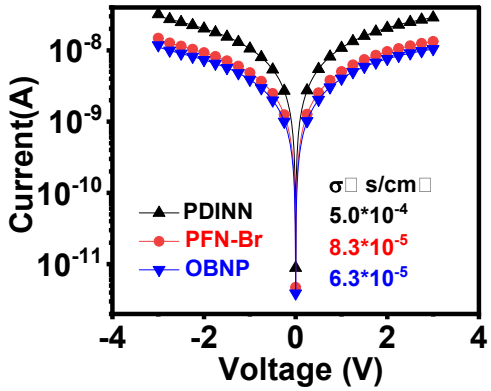

Figure S19. Current-voltage measurements and conductivity values of the three CILs.

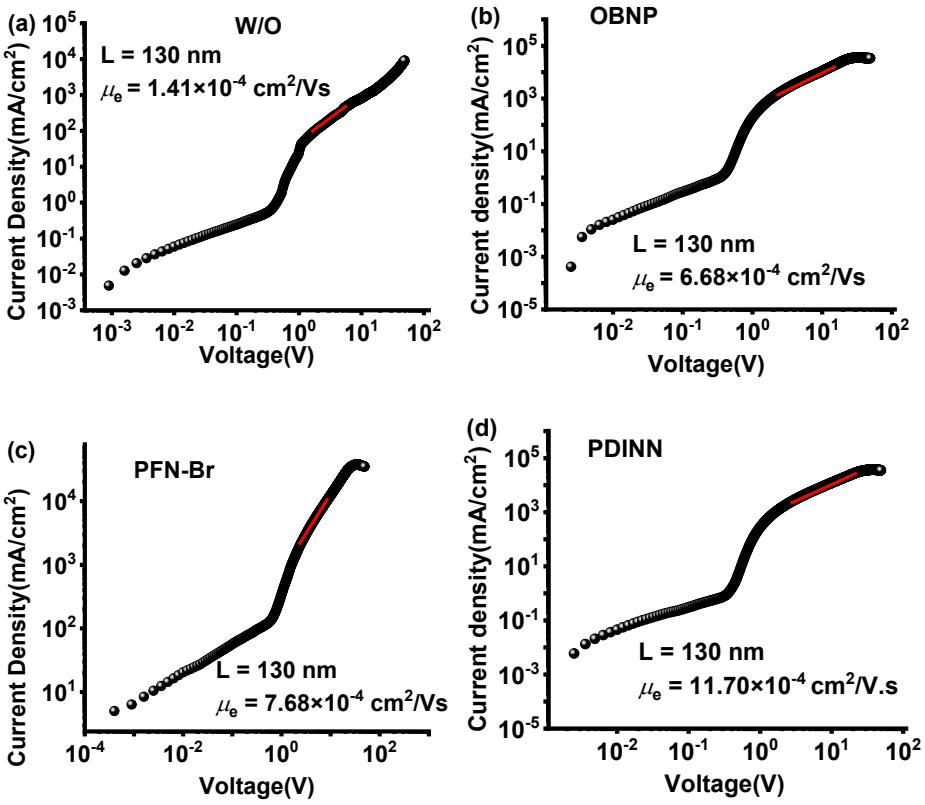

Figure S20. Electron-only SCLC plots of the devices using D18: L8-BO as active layer and different CILs of OBNP, PFN-Br, and PDINN. W/O represents the CIL-free device and the BHJ was treated by MeOH.

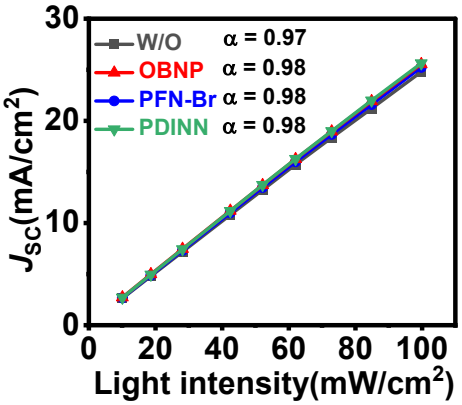

Figure S21. J_{SC}-P plots of devices using D18: L8-BO as active layer and different CILs of OBNP, PFN-Br, and PDINN. W/O represents the CIL-free device and the BHJ was treated by MeOH.

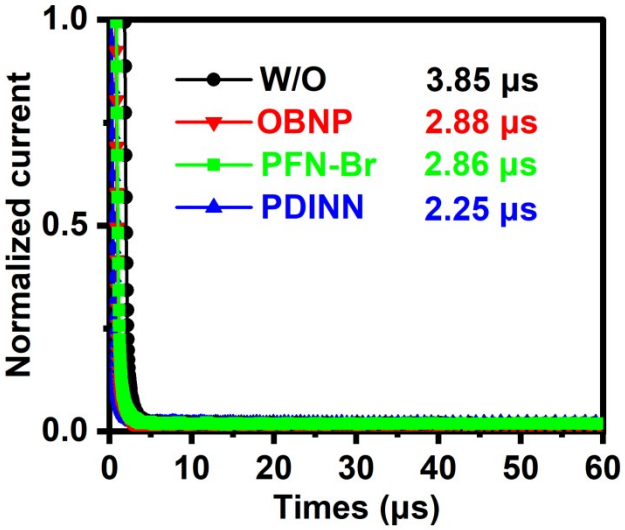

Figure S22. TPC curves of devices using D18: L8-BO as active layer and different CILs.

Table S6. The parameters of exciton dissociation efficiencies and charge collection efficiencies.

	J_{sat}[mA/cm^2]	J_{ph}^a[mA/cm^2]	J_{ph}^b[mA/cm^2]	J_{ph}^a/ J_{sat}(%)	J_{ph}^b/ J_{sat}(%)
W/O	26.83	25.51	20.06	95.08	74.77
OBNP	26.66	25.68	21.49	96.32	80.61
PFN-Br	27.02	25.94	23.33	96.00	86.34
PDINN	27.10	26.68	23.25	98.45	85.79

Notes: [a] Under short-circuit condition; [b] Under the maximal power output condition.

Table S7. Energy loss parameters of devices using D18: L8-BO as active layer and different CILs.

devices	E_g [eV]	V_{SQ} [V]	V_{rad} [V]	ΔE_1 [eV]	ΔE_2 [eV]	ΔE_3[eV][a]	ΔE_3[eV][b]	V_{OC} [V]	E_{loss}[eV][c]
W/O	1.446	1.181	1.067	0.265	0.114	0.304	0.335	0.763	0.683
PDINN	1.447	1.182	1.068	0.265	0.114	0.164	0.244	0.904	0.543
NEW	1.447	1.182	1.070	0.265	0.112	0.188	0.238	0.882	0.565

[a] Calculated from V_{rad} through the equation of $\Delta E_3 = qV_{rad} - qV_{OC}$; [b] Calculated from EQE_{EL} through the equation of $\Delta E_3 = -kT\ln(EQE_{EL})$; [c] Calculated through the equation of $E_{loss} = E_g - qV_{OC}$.

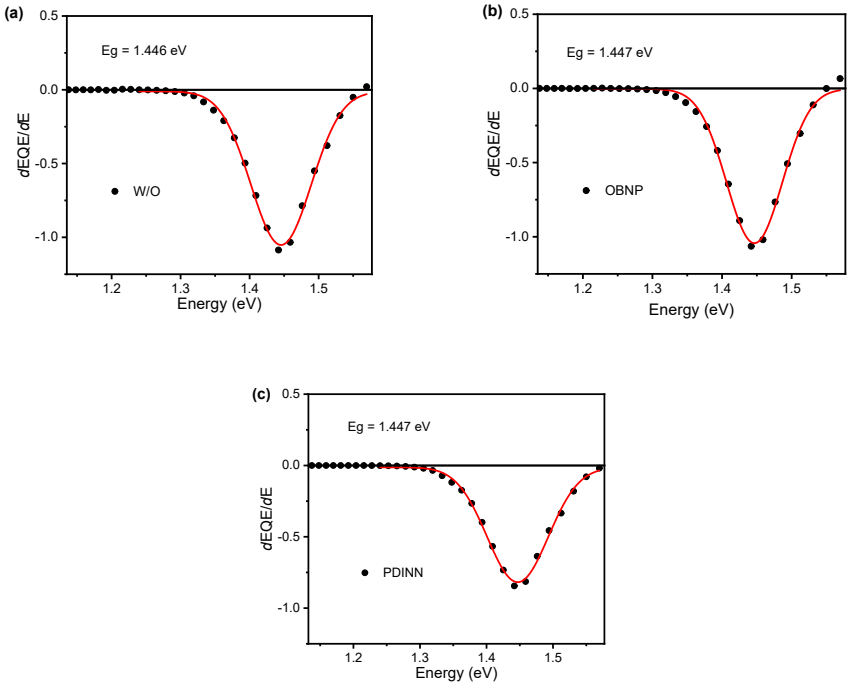

Figure S23. Optical bandgap determination of blend films on the basis of the derivatives of the sensitive EQE spectra using D18: L8-BO based devices and different CILs of W/O (a), OBNP (b) and PDINN (c).

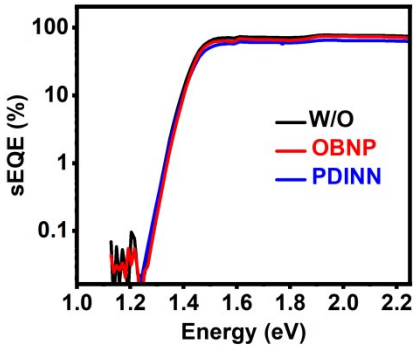

Figure S24. The sensitive EQE spectra of devices using D18: L8-BO as active layer and different CILs.

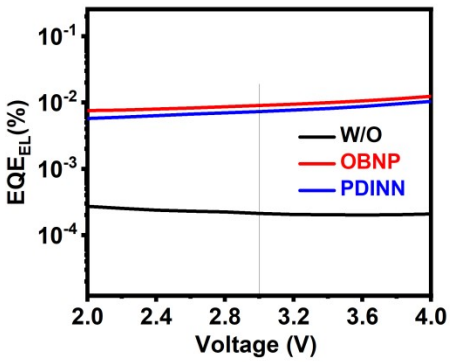

Figure S25. EQE of electroluminescence of devices using D18: L8-BO as active layer and different CILs.

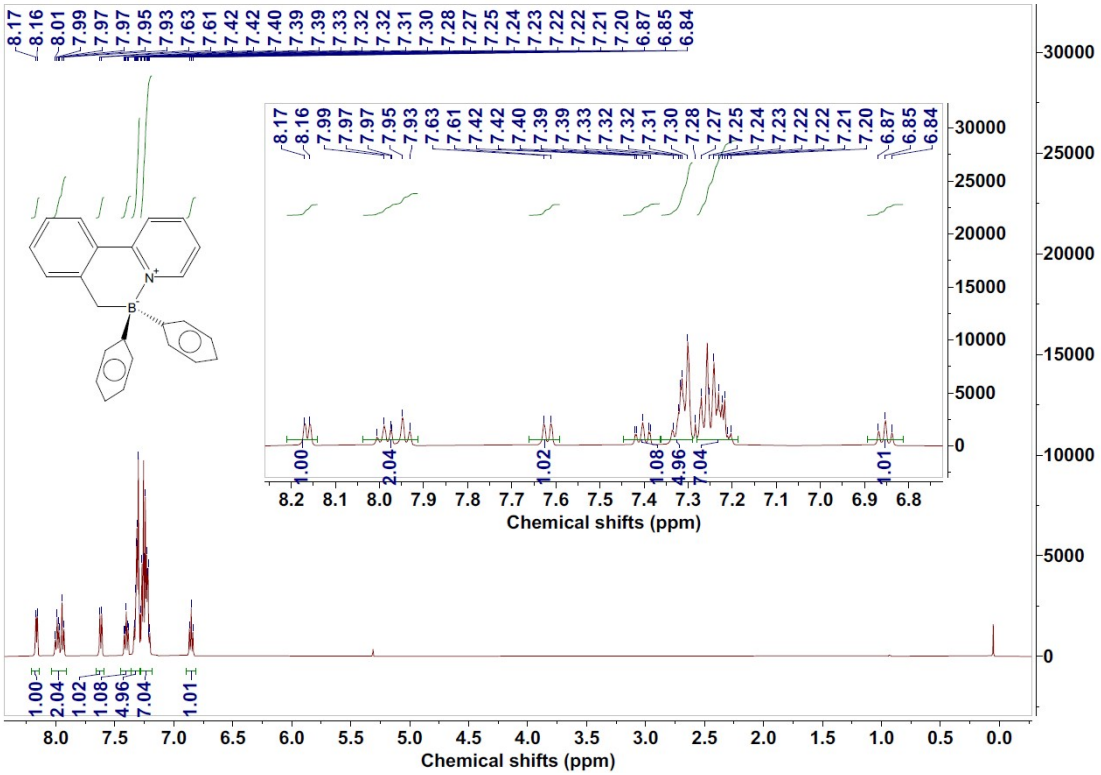

Figure S26. HNMR spectrum of OBNP.

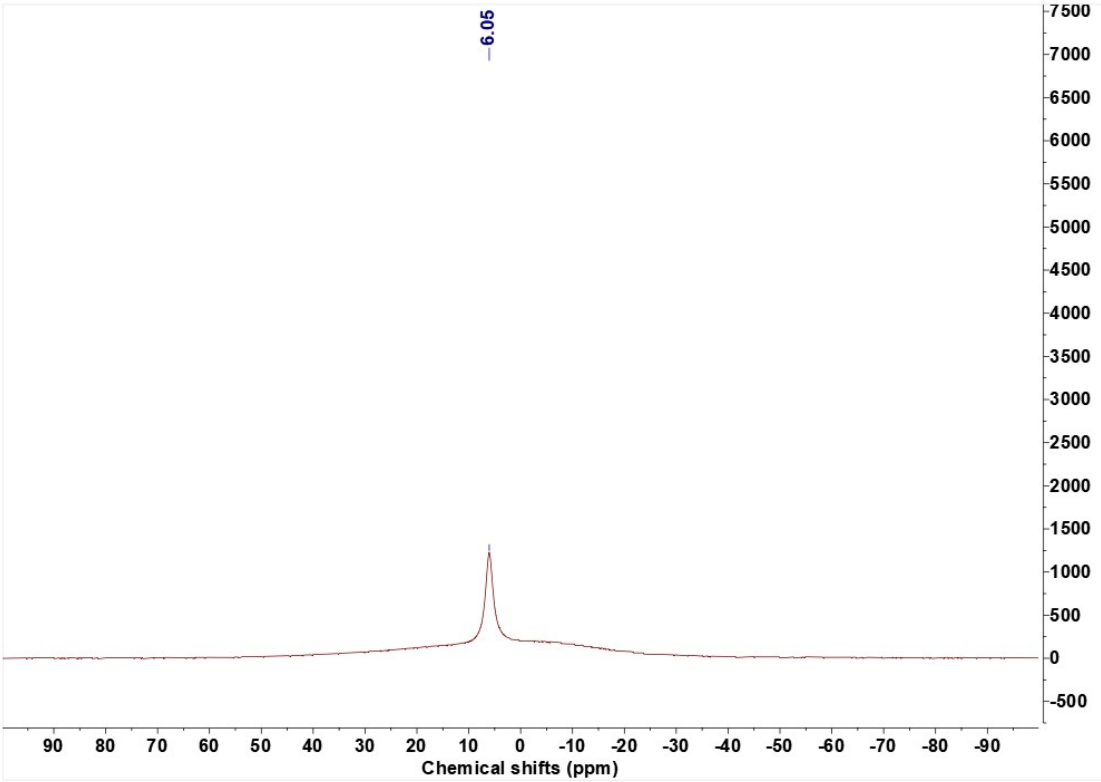

Figure S27. ^{11}B NMR spectrum of OBNP.

3 References

[1] M. J. Frisch, G. W. T., H. B. Schlegel, G. E. Scuseria, M. A. Robb, J. R. Cheeseman, J. A. Montgomery Jr., T. Vreven, K. N. Kudin, J. C. Burant, J. M. Millam, S. S. Iyengar, J. Tomasi, V. Barone, B. Mennucci, M. Cossi, G. Scalmani, N. Rega, G. A. Petersson, H. Nakatsuji, M. Hada, M. Ehara, K. Toyota, R. Fukuda, J. Hasegawa, M. Ishida, T. Nakajima, Y. Honda, O. Kitao, H. Nakai, M. Klene, X. Li, J. E. Knox, H. P. Hratchian, J. B. Cross, V. Bakken, C. Adamo, J. Jaramillo, R. Gomperts, R. E. Stratmann, O. Yazyev, A. J. Austin, R. Cammi, C. Pomelli, J. W. Ochterski, P. Y. Ayala, K. Morokuma, G. A. Voth, P. Salvador, J. J. Dannenberg, V. G. Zakrzewski, S. Dapprich, A. D. Daniels, M. C. Strain, O. Farkas, D. K. Malick, A. D. Rabuck, K. Raghavachari, J. B. Foresman, J. V. Ortiz, Q. Cui, A. G. Baboul, S. Clifford, J. Cioslowski, B. B. Stefanov, G. Liu, A. Liashenko, P. Piskorz, I. Komaromi, R. L. Martin, D. J. Fox, T. Keith, M. A. Al-Laham, C. Y. Peng, A. Nanayakkara, M. Challacombe, P. M. W. Gill, B. Johnson, W. Chen, M. W. Wong, C. Gonzalez, and J. A. Pople, Gaussian 09 (Gaussian, Inc., Wallingford CT, 2009).

[2] S. Wu, *J. Polym. Sci. C: Polym. Symp.* **1971**, 34, 19.

[3] D. Li, A. W. Neumann, *J. Colloid Interface Sci.* **1990**, 137, 304.

[4] Z. A. Tan, W. Zhang, Z. Zhang, D. Qian, Y. Huang, J. Hou, Y. Li, *Adv. Mater.* **2012**, *24*, 1476.

[5] (a) G. G. Malliaras, J. R. Salem, P. J. Brock, C. Scott, *Phys. Rev. B*, **1998**, *58*, 13411. (b) T.-Y. Chu, O.-K. Song, *Appl. Phys. Lett.*, **2007**, *90*, 203512.